

RF CHARACTERIZATION OF AN S-I-S' MULTILAYER SAMPLE

S. Keckert*, J. Knobloch, O. Kugeler, D. Tikhonov,
Helmholtz-Zentrum Berlin (HZB), Berlin, Germany

A-M. Valente-Feliciano, Thomas Jefferson National Laboratory (JLab), Newport News, USA

Abstract

S-I-S' multilayers promise to boost the performance of bulk superconductors in terms of maximum field and surface resistance. At HZB, RF-surface resistance measurements were performed with a Quadrupole Resonator (QPR) and an S-I-S' sample (75 nm NbTiN on 15 nm AlN insulator on bulk Nb) prepared at JLab. Measurements were performed at 414, 845, and 1286 MHz at sample temperatures from 2 K up to well above the transition temperature of NbTiN of ~ 17.3 K. The R_S exhibits an unexpected temperature dependence: Rather than rising monotonically, as expected from BCS theory, a local maximum is observed. There is a temperature range where R_S decreases with increasing temperature. Such behavior indicates that an additional interaction between the superconducting layers may have to be included in the surface resistance model. Measurements of the baseline Nb sample prior to coating exhibited no such behavior; hence systematic measurement errors can be excluded as the explanation. The maximum field was limited by a hard magnetic quench near 20 mT, close to H_{c1} of NbTiN, suggesting that the sample is limited by early flux penetration.

INTRODUCTION

Pushing SRF systems beyond the fundamental limits of (bulk) niobium, thin films and multilayer structures provide a promising way. Coatings of Nb₃Sn or Nb are considered as “thick” films since the deposited film thickness d is large compared to the RF penetration depth λ , justifying the assumption of one bulk-like superconductor carrying all screening currents. In thin film systems with $d = O(\lambda)$, screening currents are distributed between several layers, requiring an additional thick film or bulk superconductor underneath. Theoretical work shows that coating niobium with a superconductor of higher T_c and specific thickness, significantly increases B_{sh} and reduces the BCS surface resistance [1–3]. Inserting an insulating layer in between the superconductors prevents vortices that might be generated at defects from penetrating the entire superconducting structure.

In this work an S-I-S' structure of NbTiN and Nb with AlN as intermediate insulator was characterized using the HZB quadrupole resonator. NbTiN and AlN were deposited by DC magnetron sputtering on a bulk Nb substrate at JLab. Prior to coating, a QPR baseline test of the substrate was performed as well. In the following, the results of baseline and coated sample are discussed simultaneously to provide comparability.

* sebastian.keckert@helmholtz-berlin.de

SAMPLE PREPARATION

The sample substrate as well as the coatings were prepared at JLab. Compared to the standard sample chamber design as described in [4], this one has a slightly different mechanical design: The Nb part of sample chamber is still brazed to the stainless steel flange at the bottom. Additionally, two electron beam (EB) welds were performed. One circular weld on the RF sample surface, inserting a disk of high RRR Nb into a ring of RRR 50. This ring was then EB welded to the niobium tube that has the same low RRR. Fig. 1 shows a photo of the coated sample chamber. The high RRR disk on the RF surface was mechanically polished to mirror-like roughness. Possible contamination of the fully assembled sample setup were removed by electro-polishing. After baseline measurement at HZB, the sample was sent back to JLab, cleaned again by electro-polishing and coated afterwards. For details on the QPR at HZB refer to [4, 5].

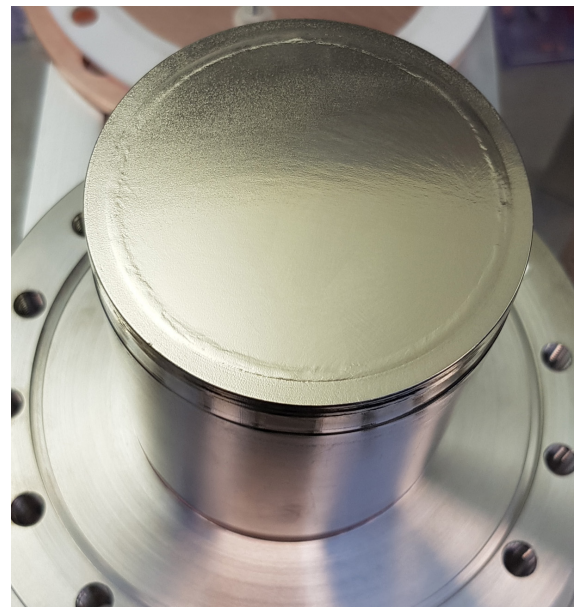


Figure 1: QPR sample with AlN and NbTiN coating on the top RF surface. Electron beam welds are visible on the top surface and on the sidewalls. The niobium tube is brazed to the stainless steel bottom flange.

After mounting into the coating chamber and evacuation to $5 \cdot 10^{-10}$ mbar, the sample was heated up to 600 °C ($p = 2 \cdot 10^{-9}$ mbar) to reduce the natural oxide layer of the niobium substrate. Sequentially, 15 nm of AlN and 75 nm of NbTiN were deposited by DC magnetron sputtering. The coating temperature was set to 450 °C to prevent diffusion of aluminum and corresponding contamination of the substrate or the top layer coating. Given by the deposition technique

and the coating chamber setup, only the top RF surface of the sample chamber and its outer edge are covered by the S-I layers.

SURFACE RESISTANCE

Baseline Measurement

Prior to the coating process, a baseline surface resistance measurement of the bulk niobium substrate was performed at 414 and 846 MHz. BCS fits according to the empirical expression

$$R_S(T) = \frac{a}{T} \left(\frac{f}{414 \text{ MHz}} \right)^2 \exp\left(-\frac{\Delta}{kT}\right) + R_{\text{res}} \quad (1)$$

were calculated. The resulting residual resistance as a function of the applied RF field strength is shown in Fig. 2. Measurement data as a function of temperature is shown later, together with the one obtained for the coated sample (see Fig. 4a).

R_{res} is nearly independent of RF field for both frequencies. Assuming a field independent scaling factor of $73/23 \approx 3.2$ corresponds to a frequency dependence of $R_{\text{res}} \propto f^{1.63}$. Similar scaling has been observed on multi-mode test cavities before and seems typical for bulk niobium [6, 7]. The absolute values however indicate non-ideal behavior, scaling to a 1.3 GHz TESLA-shaped cavity yields $R_{\text{res}} = 150 \text{ n}\Omega$ and $Q_0 = 1.8 \cdot 10^9$. The residual resistance might be due to increased losses on the outer 'ring' of the sample. As mentioned above, only the inner 'disk' of the sample surface is made of high quality high RRR niobium. Given by the high temperatures during electron beam welding, the 'ring' may have contaminated the 'disk' due to diffusion. In the case of such an inhomogeneity, the true residual resistance of the outer ring would be even higher, since the calorimetric measurement principle always gives a surface average value. Note that the fit uncertainty indicated by semi-transparent areas in Fig. 2 is dominated by the systematic RF measurement uncertainty of 9.2%. This is mainly relevant when comparing different frequencies since RF calibration errors systematically shift the entire data set obtained at one quadrupole mode. For a detailed discussion of errors impacting fit parameters see [8].

After subtracting an RF field independent residual resistance of 23 nΩ (Q1, 414 MHz), resp. 73 nΩ (Q2, 846 MHz) from measurement data, the temperature dependent BCS resistance is shown as a function of RF field in Fig. 3. At low fields of 10 and 20 mT the data perfectly matches the expectation of $B_{\text{BCS}} \propto f^2$. Reversely, this excludes significant frequency specific, systematic errors of the RF measurement system. Towards higher RF field, the increase of R_{BCS} is suppressed at higher frequency.

S-I-S' NbTiN-AlN-Nb Sample

Measurement data for surface resistance vs. sample temperature is shown in Fig. 4a for both, baseline and S-I-S' sample. For the S-I-S' sample, $R(T)$ curves at all three frequencies show suspicious behavior that is both significant

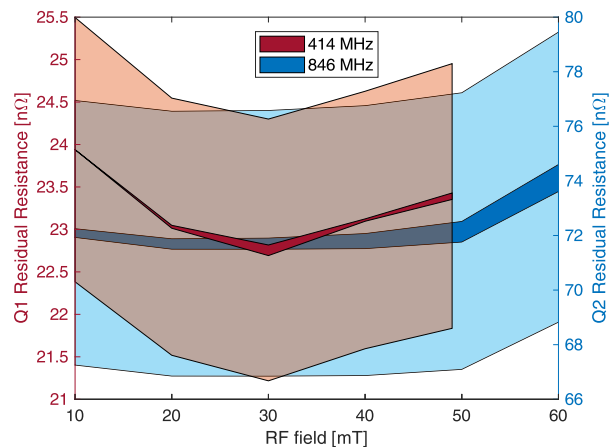


Figure 2: Baseline residual resistance R_{res} obtained from fitting $R_S(T)$ curves for different values of RF field at frequencies of 414 and 845 MHz. Dark colored areas indicate the fit stability when changing of upper limit. Semi-transparent areas give the fit uncertainty including the systematic RF uncertainty.

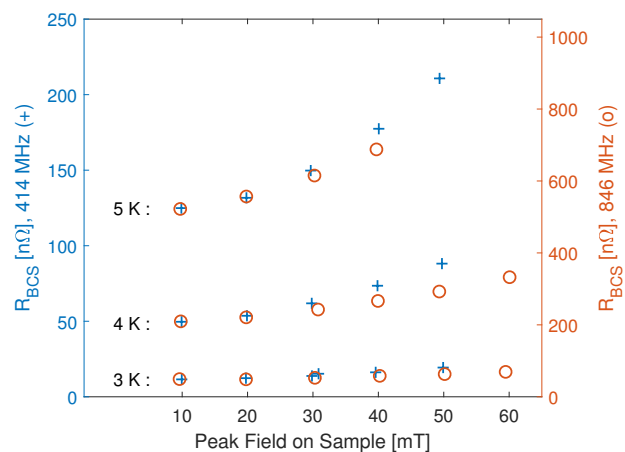
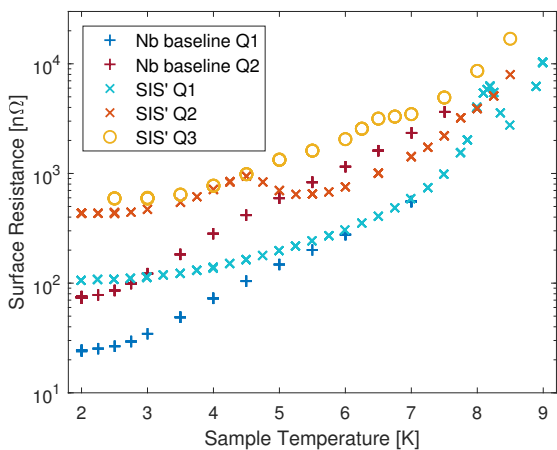


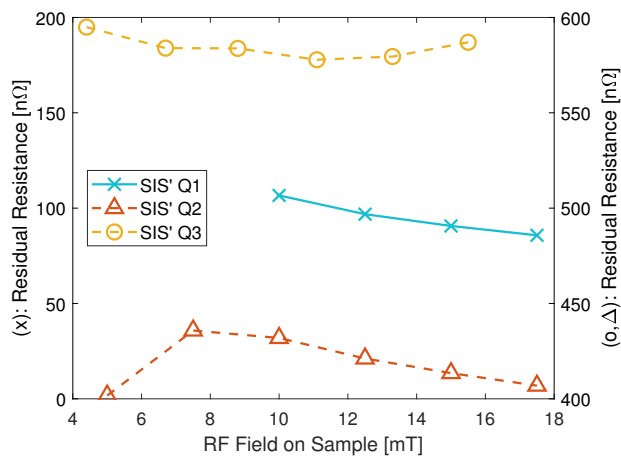
Figure 3: Temperature dependent BCS surface resistance vs. RF field on sample for the baseline measurement. The values were calculated by subtracting an RF field independent residual resistance of 23 nΩ (414 MHz), resp. 73 nΩ (846 MHz) from measurement data (see Fig. 2). Note that the y-axes are linked quadratically by $(846/414)^2 \approx 4.2$.

and reproducible. At Q1 (414 MHz) and Q2 (845 MHz) a region of non-monotonic dependence on temperature is observed, each featuring a distinct local minimum that differs in position and width. At Q1, comparable values of surface resistance are obtained at temperatures of 8.2 and 8.9 K, indicating a local minimum near 8.55 K. An interjacent decrease of more than 50% is recorded. For Q2 this minimum lies near 5.4 K with a width of about ± 0.9 K. The decrease of 300 nΩ (or 30%) is less pronounced than at Q1. For the third quadrupole mode less data points are available. However, a decrease spanning several Kelvin can be excluded while a change of slope is visible in between 6.5 and 7 K.

Content from this work may be used under the terms of the CC BY 3.0 licence (© 2019). Any distribution of this work must maintain attribution to the author(s), title of the work, publisher, and DOI.

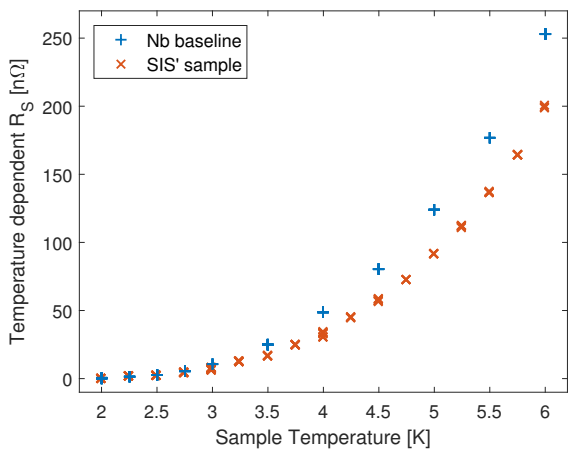


(a) Measured R_S

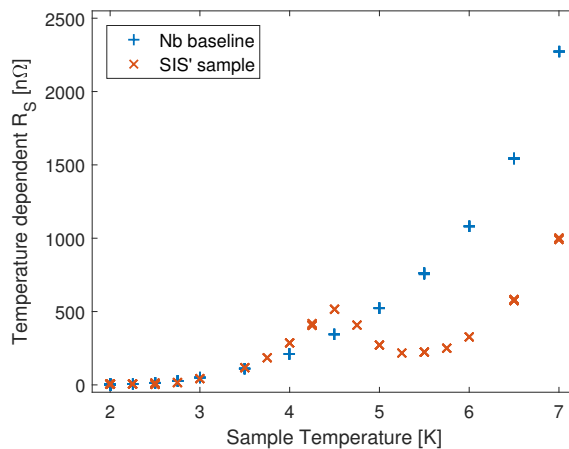


(b) Residual resistance

Figure 4: (a) Measured surface resistance vs. sample temperature for baseline and S-I-S' measurement. All points at QPR modes Q1 and Q2 were taken at $B_{RF} = 10$ mT, for Q3 $B_{RF} = 8.8$ mT. (b) S-I-S' temperature independent residual resistance as a function of RF field. The right-hand y-axis for data points at Q2 and Q3 is shifted but has the same steps as the left-hand axis. For baseline R_{res} see Fig. 2.

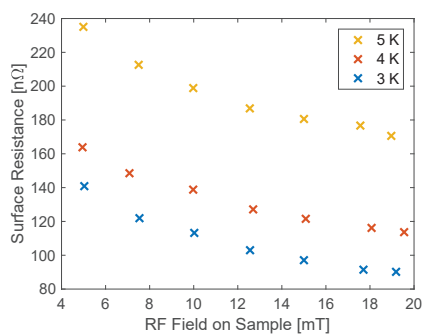


(a) Q1, 414 MHz

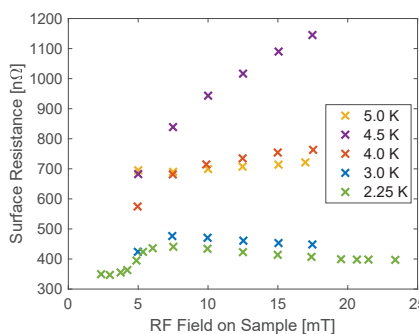


(b) Q2, 845–846 MHz

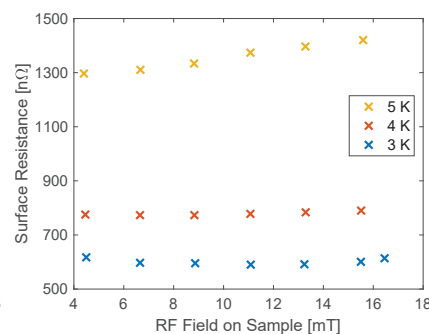
Figure 5: Temperature dependent surface resistance vs. sample temperature for baseline and S-I-S' measurement after subtraction of R_{res} according to Figs. 2 and 4b. All points were taken at $B_{RF} = 10$ mT.



(a) 414 MHz



(b) 845 MHz



(c) 1286 MHz

Figure 6: Surface resistance vs. RF field for the S-I-S' sample. For baseline measurement data see Fig. 3.

Note that an increasing contribution of the niobium substrate is expected at elevated temperatures since the S-I coatings do not cover the sidewalls of the sample chamber. However, this contribution is strictly monotonic in temperature and cannot explain the observed features.

In the following, the partition of measured surface resistance into residual and BCS contribution for investigating $R(T)$ might be arguable. For that reason, the BCS approximation given by Eq. (1) is used only to extrapolate a temperature independent residual resistance. This is justified due to the fact that for a certain low-temperature range, both RMSE and R_{res} values vary reasonably low when changing the fit data range. Resulting values are shown in Fig. 4b. Compared to the baseline measurement, a strong increase of residual resistance is observed. However, the rise of surface resistance with temperature is suppressed, which is expected given the comparatively high T_c of NbTiN. At the first quadrupole mode, this becomes clearly visible after subtracting R_{res} from the measurement data (see Fig. 5a).

For Q2 the effect of non-monotonic $R(T)$ “overcompensates” the higher R_{res} , leading to a lower total surface resistance than for baseline niobium for $T \gtrsim 5.2$ K. Subtracting R_{res} yields the contradicting picture of higher temperature dependent surface resistance in the range of ~ 3.5 to 4.7 K than for bulk niobium (see Fig. 5b). Hence, the observed local minimum of $R(T)$ is more likely a consequence of a temperature range with strongly enhanced surface resistance, than of a mechanism reducing R_S . A mechanism of enhanced losses also fits to the visual impression of $R(T)$ at Q1 in the temperature range of 7.8 to 8.5 K. At the peak, the measured R_S even exceeds the data obtained at 845 MHz (Q2). Furthermore, such a mechanism could explain the comparatively small change in surface resistance when increasing the frequency from Q2 to Q3 (see Fig. 4a): Continuing the trend of a peak in R_S at T_{pk} , and assuming that T_{pk} decreases with frequency might lead to $T_{\text{pk}} < 2.5$ K at Q3 (1286 MHz). Unfortunately, surface resistance measurements were impossible in this temperature range due to high RF heating. Hence, the value of $R_{\text{res}} = 584$ n Ω could be affected significantly. Remember, so far we only investigated data measured at constant RF field of $B_{\text{RF}} = 10$ mT (8.8 mT in case of Q3).

The measured surface resistance as a function of RF field is given in Fig. 6. Again, significantly different behavior is observed when changing the frequency. At the second quadrupole mode, a detailed two-dimensional measurement data grid was possible, as shown in Fig. 7. Intersections of the black grid lines denote measured data points, the color representation is interpolated for better readability. At Q1, the surface resistance consistently decreases towards higher field. At low temperatures of 3 and 4 K this effect is stronger than the increase of $R_S(T)$. This requires an RF field dependent residual – or, more precise, temperature independent – resistance, as visible in Fig. 4b. At Q2, a similar but quantitatively smaller decrease of surface resistance with RF field is restricted to field levels larger than 7.5 mT and temperatures below 3.5 K. Approaching the local peak in R_S at 4.5 K yields a surface resistance growing with field. For higher

temperatures ($T \gtrsim 5$ K), R_S depends only slightly on field. For Q3, the surface resistance also depends slightly on RF field with a tendency of increasing Q-slope towards higher temperature.

As for the curves of $R(T)$, the behavior of $R(B)$ changes at or near the characteristic temperature $T_{\text{pk}}(f)$. This allows a single mechanism which consistently describes the deviation from expected BCS-behavior at all three frequencies: For $T \ll T_{\text{pk}}$ the surface resistance decreases with field. Near T_{pk} , R_S increases with RF field, while it becomes nearly independent of the applied RF field strength for $T \gg T_{\text{pk}}$. The value of T_{pk} itself decreases for higher frequency and causes a distinct temperature range with enhanced surface resistance. Note that this mechanism also includes RF field dependent residual resistance.

The physical reason for this behavior is still unclear. One possibility might be a quantum mechanical coupling of the two superconducting layers. For this sample, the insulator thickness of 15 nm is about three times the coherence length of NbTiN but significantly smaller than $\xi_{0,\text{Nb}} = 39$ nm. Further measurements to study the dependence of $R(T, B, f)$ on the insulator thickness are ongoing.

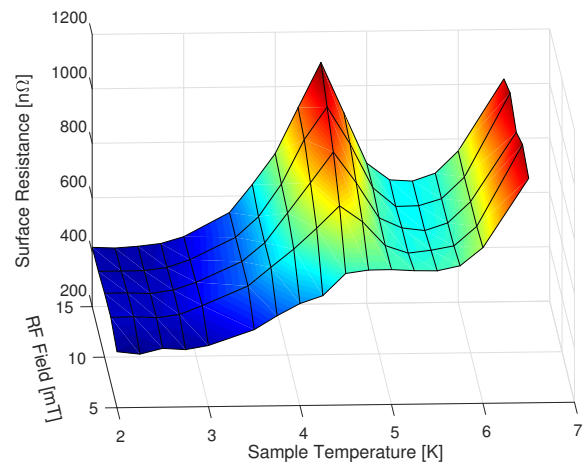


Figure 7: Measured R_S vs. sample temperature and RF field strength at 845 MHz for the S-I-S’ sample. Intersections of the black grid lines denote measured data points, colors are interpolated for better readability.

PENETRATION DEPTH

In an SRF cavity, the superconducting penetration depth of the used material can be deduced from measuring the resonant frequency shift as a function of temperature. Thanks to the thermal decoupling of sample and surrounding cavity in case of the QPR, this directly gives the penetration depth of the sample material. However, for use with the well-known formula

$$\Delta\lambda = \lambda(T) - \lambda_0 = -\frac{G_{\text{Sample}}}{\pi\mu_0 f_0^2} \Delta f \quad (2)$$

a single-valued penetration depth has to be defined. In analogy to the simple case of $B(x) \propto \exp(-x/\lambda)$ and

$\lambda = \int_0^\infty \exp(-x/\lambda) dx$, the effective value λ_{eff} is defined as

$$\lambda_{\text{eff}}(T) = \frac{1}{B(T, x=0)} \int_0^\infty B(T, x) dx. \quad (3)$$

$B(x)$ is calculated using the analytic expression of [3], with temperature dependence of the individual layers according to the Gorter-Casimir expression

$$\lambda(T) = \frac{\lambda_0}{\sqrt{1 - \left(\frac{T}{T_c}\right)^4}}. \quad (4)$$

For simplicity, the integration is calculated numerically in the range of $x = 0 - 5 \mu\text{m}$ with variable resolution of $dx = 0.1 \text{ nm}$ for $x \leq 500 \text{ nm}$ and $dx = 0.5 \text{ nm}$ for $x > 500 \text{ nm}$. When exceeding the critical temperature of a layer, λ_i is replaced by the normal conducting skin depth δ_{nc} . Normal state resistivities are taken from literature with $\sigma_{\text{Nb,RT}} = 6.58 \cdot 10^6 \text{ S/m}$ and $\sigma_{\text{NbTiN,cryo}} = 2.86 \cdot 10^6 \text{ S/m}$ [9]. For niobium, σ_{RT} is further increased by its RRR.

Ideally, the contribution of niobium can be described by T_c and RRR only, with the latter yielding both, $\lambda(T)$ and δ . However, depending on $T < T_{c,\text{Nb}}$ or $T > T_{c,\text{Nb}}$, a very different sample volume is probed by the RF field. Especially the substrate purity (RRR, ℓ) can change significantly and furthermore impacts the fit curve in the entire temperature range. Hence, superconducting RRR_{sc} and normal conducting δ_{nc} are fit individually, allowing for a vertical change in purity of the niobium substrate.

In order to reduce coupled uncertainties and the number of free parameters, the values of ξ_1 and $\lambda_{L,i}$ for each (superconducting) layer are fixed. Furthermore, an iterative fit procedure is applied: The critical temperatures are determined in preliminary fit runs, in case of $T_{c,\text{Nb}}$ the data range is restricted to $T < 9.25 \text{ K}$. Subsequently, the parameters RRR_{sc} , δ_{nc} and λ_0 are obtained using a global fit to the full temperature range of $4 - 18 \text{ K}$. Measurement data for the S-I-S' sample at all three quadrupole modes is shown in Fig. 8, corresponding fit results can be found in Table 1. The measurements were done by performing frequency scans with a computer-controlled vector network analyzer [10]. Individual thermal cycles were carried out for the three quadrupole modes.

The critical temperature of the niobium substrate is found throughout all three frequencies in very good agreement with the expectation from literature of $T_{c,\text{Nb}} = 9.25 \text{ K}$. The superconducting RRR_{sc} – or more precisely its value for the uppermost $\approx 100 \text{ nm}$ – scatters strongly but the weighted average of $\text{RRR}_{\text{sc}} = 42 \pm 8$ is consistent within the big statistical fit uncertainty for all three values. Note that in the superconducting state the penetration depth should be independent on frequency. The observed scatter together with the absolute values can hence be interpreted as an indication for compositional inhomogeneities, e. g. part of the deposited coating could be diffused into the RF layer of the substrate, explaining the comparatively low values of RRR_{sc} . In contrast to that, RRR_{nc} has no clear dependence

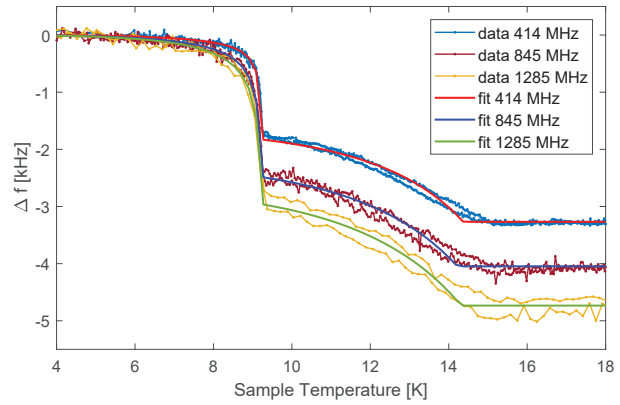


Figure 8: Measured frequency shift vs. sample temperature for all three quadrupole modes. Fits using Eq. (3) are shown with solid lines, result data is given in Table 1.

on frequency, even though being obtained from significantly different depths x of the probed sample volume. Hence, for $x \gtrsim 200 \text{ nm}$, i. e. below the region of sc RF currents, the niobium substrate is found to be homogeneous and of high purity. This is consistent with the expectation of $\text{RRR} \gtrsim 300$ from the used sheet material.

For the NbTiN top layer very consistent results are obtained for all three frequencies. The result of $\lambda(0 \text{ K}) \approx 246 \text{ nm}$ is higher than literature values of $\lambda = 150 - 200 \text{ nm}$ [9] but can be explained by a reduced mean free path due to the film deposition technique. The observed critical temperature of about 14.3 K is significantly lower than expected (confer 17.3 K [9]). This indicates issues of the coating that might be a reason for the very high residual resistance compared to the baseline measurement, or the small critical field.

CRITICAL FIELD

The RF quench field of the bulk niobium substrate was obtained in the baseline measurement using the single pulse technique at 414 and 846 MHz as described in [10]. Experimental data is shown in Fig. 9 together with fits according to the empirical expression

$$B_c(T) = B_0 \cdot \left(1 - \left(\frac{T}{T_c}\right)^2\right). \quad (5)$$

For quantitative fit results see Table 2. The temperature range used for fitting is shown by solid lines, dashed lines indicate the extrapolation to 0 K . Fit results of $B_0 \approx 220 - 250 \text{ mT}$ are in very good agreement with the expected superheating limit for niobium. However, a strictly quadratic dependence on temperature is observed only at high temperatures, the sample could exhibit reduced quench fields at lower temperature. Unfortunately, the QPR quench limit ruled out further measurements in that range.

For the S-I-S' sample, first hints for a low RF quench field were observed during surface resistance measurements: The measured R_s jumped up suddenly when exceeding a field

Table 1: S-I-S' Penetration Depth Measurement. Error bars give statistical fit errors.

	Frequency	414 MHz	845 MHz	1265 MHz
bulk Nb substrate	$T_{c, Nb}$	9.26 ± 0.01 K	9.28 ± 0.04 K	9.29 ± 0.08 K
	$\lambda(0$ K)	46 ± 2 nm	50 ± 2 nm	44 ± 4 nm
	δ_{nc}	515 ± 4 nm	378 ± 3 nm	299 ± 6 nm
	λ_L		32 nm (fixed)	
	ξ_0		39 nm (fixed)	
	RRR _{sc}	21 ± 4	15 ± 2	25 ± 10
	RRR _{nc}	350 ± 5	319 ± 5	335 ± 12
NbTiN layer	$T_{c, NbTiN}$	14.37 ± 0.03 K	14.22 ± 0.05 K	14.32 ± 0.13 K
	$\lambda(0$ K)	246 ± 2 nm	248 ± 3 nm	237 ± 6 nm
	δ_{nc}	14.63 μ m	10.24 μ m	8.30 μ m
	ξ_0		5 nm (fixed) [9]	
	κ	49.1 ± 0.4	49.6 ± 0.5	47.3 ± 1.2

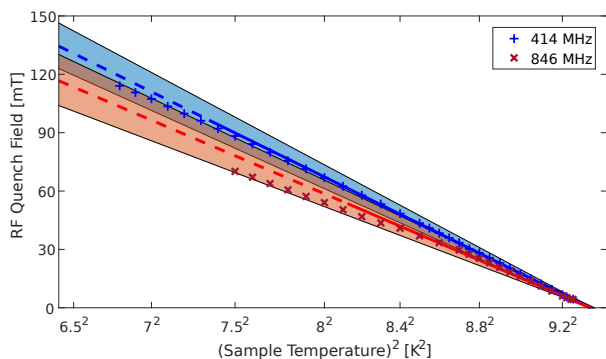


Figure 9: Baseline RF quench field of the bulk Nb substrate. Semi-transparent areas give the total fit uncertainty, which is dominated by the systematic uncertainty of the RF system. Fit parameters are given in Table 2.

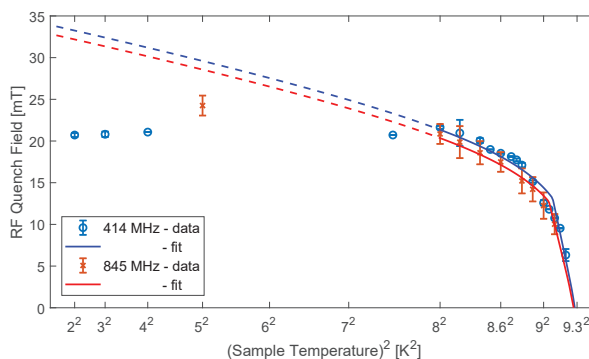


Figure 10: RF quench field of the S-I-S' sample, measured at 414 and 845 MHz. Fit parameters are given in Table 2. The error bars give statistical uncertainty and reproducibility only, 6.5 % of relative systematic RF uncertainty has to be added.

level of about 20 mT. This behavior consistently occurred for CW and pulsed RF power, which indicates both, good thermal connection to the substrate and a “magnetic” origin of the quench. Thermal runaway – even accelerated by observed the Q-slope – can be excluded: Given the long thermal path of the QPR sample chamber, the RF sample can be operated “on the edge” where such a runaway occurs. Increasing the RF field by few μ T will then trigger a “slow” runaway that takes several seconds for a temperature rise of the order of Kelvins. Much higher fields, of course, will lead to fast thermal quenches that can not be resolved in time domain by eye. However, for this sample, very stable sample temperature (and surface resistance data) was obtained close to the quench point with instantaneous jumps of several Kelvin (or $\mu\Omega$) when slightly increasing the RF field.

For quantitative investigation of the RF quench field, the single pulse technique was applied again at 414 and 845 MHz. Measurement data is shown in Fig. 10. Non-linear fits use the expression of [3], including the temperature dependencies of λ_i and $B_{sh,i}$ for each layer. For simplicity, the empirical quadratic dependence on temperature of Eq. (5) is used for $B_{sh,i}$. Resulting fit parameters are given in Table 2.

The temperature axis of Fig. 10 is scaled quadratically to improve readability at high temperature. Note that for S-I-S' structures non-linear behavior is expected in this representation.

The data confirms an RF quench field in the range of 20 to 25 mT which is even below the lower critical field of $H_{c1, NbTiN} = 30$ mT [9]. Measurements at 414 and 845 MHz are consistent within the measurement uncertainty. Fits are shown by solid lines and extrapolated to low temperature as indicated with dashed lines. Near 9.1 K the transition of the quenching top layer ($T < 9.1$ K) to the quenching substrate ($T > 9.1$ K) is visible. Below 8 K the observed RF quench field does not depend on temperature as expected but stays nearly constant. This is interpreted as additional non-fundamental quench limitation, possibly due to local defects with early vortex penetration.

The fitted temperature range contains only few data points on each curve. In order to prevent overfitting with unphysical results, only $T_{c, Nb}$ and $B_{0, NbTiN}$ are fitted, all other parameters were fixed to the results of the penetration depth measurement (see Table 1). The RF field limit for the niobium substrate is taken from the baseline measurement.

Content from this work may be used under the terms of the CC BY 3.0 licence (© 2019). Any distribution of this work must maintain attribution to the author(s), title of the work, publisher, and DOI.

For the NbTiN layer a low-temperature quench field of $B_{0,NbTiN} \approx 17$ mT is obtained at both frequencies. This is about half of $H_{c1,NbTiN}$ and far below the expected superheating limit of $H_{sh,NbTiN} \approx 440$ mT [11]. Coating flaws as already suspected from the high residual surface resistance and the low critical temperature would also explain these values as well as early vortex penetration.

The DC magnetic field of first vortex penetration was measured for a witness sample that was coated together with the QPR sample. The result of $B_{vp} = 15\text{--}20$ mT is very close to the observed RF quench field but far less than expected for such film thickness. A witness sample prepared under comparable conditions with slightly increased thicknesses of 80 nm NbTiN and 20 nm AlN showed $B_{vp} = 160$ mT. Further measurements on the coating characteristics are ongoing.

Table 2: Fit Results of the Critical Field Measurements for the Bulk Nb Substrate (Baseline) and the S-I-S' Sample

	Frequency	$B_{0,Nb}$ [mT]	$T_{c,Nb}$ [K]
Nb	414 MHz	250 ± 20	9.33 ± 0.01
	846 MHz	220 ± 24	9.34 ± 0.01
	Frequency	$B_{0,NbTiN}$ [mT]	$T_{c,Nb}$ [K]
S-I-S'	414 MHz	17.2 ± 1.9	9.28 ± 0.03
	845 MHz	17.0 ± 1.7	9.27 ± 0.04

CONCLUSION

In summary, a first successful measurement campaign of an S-I-S' sample using a quadrupole resonator together with quantitative analysis using recent theoretical methods is reported. Surface resistance data is available at frequencies of 414, 845 and 1286 MHz, in the temperature range of 2 – 9 K. The RF quench limit restricted measurements to $B_{RF} \lesssim 23$ mT. $R(T)$ data at Q1 and Q2 shows non-monotonic behavior with local maxima at $T_{pk,Q1} = 8.2$ K and $T_{pk,Q2} = 4.5$ K. Near this characteristic temperature the dependence of R_S on the RF field changes as well. For $T \ll T_{pk}$, total and residual surface resistances decrease towards higher field; while at T_{pk} a strong increase of R_S with field is observed. Continuing the trend of T_{pk} decreasing with frequency might lead to $T_{pk} < 2.5$ K at Q3, which was not detectable because of too high RF heating. In that case, the extrapolated surface resistance could be affected significantly. A possible physical reason for this behavior could be a coupling of the two superconducting layers. The insulator thickness of 15 nm is about three times the coherence length of NbTiN but significantly smaller than $\xi_{0,Nb} = 39$ nm. In this case the theoretical models of [2, 3] that were used throughout this work should be revised. Such a coupling mechanism would impact the applicability of multilayer structures for SRF systems significantly. Further measurements to study the dependence of $R(T, B, f)$ on the insulator thickness are ongoing.

The performance of the current coatings is very likely limited by non-fundamental issues: The observed critical

temperature of $T_{c,NbTiN} \approx 14.3$ K is significantly lower than expected and R_{res} is clearly higher than for the niobium baseline measurement. The temperature-independent RF quench field for $T < 8$ K indicates early vortex penetration, which occurs preferentially at weakly superconducting locations, e. g. at defects or spots of wrong composition. In that case, single or few quench spots limit the global performance while the surface averaging penetration depth measurement is far less sensitive to small-sized effects.

REFERENCES

- [1] A. Gurevich, "Enhancement of rf breakdown field of superconductors by multilayer coating," *Applied Physics Letters*, vol. 88, no. 1, p. 012511, 2006. doi: 10.1063/1.2162264.
- [2] A. Gurevich, "Maximum screening fields of superconducting multilayer structures," *AIP Advances*, vol. 5, no. 1, p. 017112, 2015. doi: 10.1063/1.4905711.
- [3] T. Kubo, "Multilayer coating for higher accelerating fields in superconducting radio-frequency cavities: A review of theoretical aspects," *Superconductor Science and Technology*, vol. 30, no. 2, p. 023001, 2016. doi: 10.1088/1361-6668/30/2/023001.
- [4] R. Kleindienst, O. Kugeler, and J. Knobloch, "Development of an optimized quadrupole resonator at hzb," in *Proc. of the 16th International Conference on RF Superconductivity (SRF'13), Paris, France, 2013*, pp. 614–616. <http://accelconf.web.cern.ch/AccelConf/SRF2013/papers/tup074.pdf>
- [5] R. Kleindienst, A. Burrill, S. Keckert, J. Knobloch, and O. Kugeler, "Commissioning Results of the HZB Quadrupole Resonator," in *Proc. of International Conference on RF Superconductivity (SRF'15), Whistler, BC, Canada, 2015*, 2015, pp. 930–936, ISBN: 978-3-95450-178-6. doi: 10.18429/JACoW-SRF2015-WEA1A04.
- [6] P. Kneisel, O. Stoltz, and J. Halbritter, "Investigation of the surface resistance of a niobium-cavity at s-band," *IEEE Transactions on Nuclear Science*, vol. 18, no. 3, pp. 158–159, 1971, ISSN: 0018-9499. doi: 10.1109/TNS.1971.4325993.
- [7] P. Kneisel, "Radio-frequency superconductivity technology: Its sensitivity to surface conditions," *Journal of Vacuum Science & Technology A: Vacuum, Surfaces, and Films*, vol. 11, no. 4, pp. 1575–1583, 1993. doi: 10.1116/1.578507.
- [8] S. Keckert, J. Knobloch, and O. Kugeler, "Error Analysis of Surface Resistance Fits to Experimental Data," in *Proc. of International Conference on RF Superconductivity (SRF'17), Lanzhou, China, 2017*, 2018, pp. 859–862, ISBN: 978-3-95450-191-5. doi: 10.18429/JACoW-SRF2017-THPB052.
- [9] A.-M. Valente-Feliciano, "Superconducting RF materials other than bulk niobium: A review," *Superconductor Science and Technology*, vol. 29, no. 11, p. 113002, 2016. doi: 10.1088/0953-2048/29/11/113002.
- [10] S. Keckert, Ph.D. thesis, to be submitted.
- [11] T. Junginger, T. Prokscha, Z. Salman, A. Suter, and A.-M. Valente-Feliciano, "Critical Fields of SRF Materials," in *Proc. 9th International Particle Accelerator Conference (IPAC'18), Vancouver, BC, Canada, 2018*, 2018, pp. 3921–3924, ISBN: 978-3-95450-184-7. doi: 10.18429/JACoW-IPAC2018-THPAL118.